EXPERIMENTAL CHARACTERISATION AND COMPARISON OF A MODEL HELICOPTER ROTOR TIP VORTEX AND FIXED WING TIP VORTEX

T Denton, J Martins, G Ratner, and P Skinner
Defence Aeronautics Programme, Defencetek, CSIR

tdenton@csir.co.za, jmartins@csir.co.za, gratner@csir.co.za, pskinner@csir.co.za

Abstract

Interference effects of trailing vortices from aircraft have implications for the safe operation of following aircraft. This paper presents the first phase of an investigation into the interference effects of rotorcraft vortices. In this phase, the trailing vortex characteristics of a model rotor and those of a fixed wing were measured experimentally in the Seven Metre Wind Tunnel at the CSIR in South Africa.

The tests on the rotorcraft vortices were carried out using a radio controlled model of an Agusta 109 helicopter, with a fully articulated four bladed main rotor of 1337 mm diameter. A 1200 mm span, NACA 0012 profile wing, with a chord of 200 mm was tested at similar lift values to those obtained during the rotor tests. A three-wire orthogonal hot-wire probe was used for the measurement of the wake characteristics.

Wing and rotor data was compared in terms of vortex strength, tangential velocity, and radius for a representative flight condition. The vortex structure of the wing was compared to results obtained by Corsiglia et al[2].

The trailing vortex data captured for the wing was successfully compared with published data and with data from the rotor. Significant differences between the wing and the rotor trailing vortex structures were identified.

Nomenclature

A, B, C, D, E = Empirical constants

AR = Aspect Ratio

b = Wing Span, m

c = Chord, m

C_L = Lift Coefficient

d = Rotor Diameter, m

r = Radial Coordinate from Vortex Centre, m

r_0 = Outer Radius, where $\Gamma = 0.99\ \Gamma_0$, m

r_1 = Radial position of maximum tangential velocity, m

V_∞ = Wind Tunnel Free Stream Velocity, m/s

V_θ = Tangential Velocity, m/s

α = Angle of Attack, ∞

Γ = Circulation around a Contour of Radius r ($=2\pi r V_\theta$), m≤s

Γ_0 = Value of Circulation Shed from One Side of the Wing or Rotor, m≤s

Γ_1 = Value of Circulation at position of maximum tangential velocity, m≤s

Introduction

This work was co-funded by the AMRDEC (Aviation and Missile Research, Development and Engineering Center (US Army Aviation and Missile Command)) group of the US Army, through the European Research Office of the US Army. The work was carried out under the leadership of Dr C Tung of AMRDEC.

Many studies have been previously carried out to measure and understand the trailing vortex structure of fixed wing aircraft, and the interference effects on following aircraft. This is, however, not the case for rotorcraft.

A significant amount of research has been carried out on the measurement of rotor wakes but these have focussed on near wake characteristics. The most extensive downstream rotor wake measurements identified in the literature were those described by Ghee et al[1] in which rotor wake measurements were taken up to 2 rotor diameters downstream. Such studies have been carried out experimentally to quantify the wake parameters of helicopter rotors for comparison with computational predictions of the wake parameters. These investigations did not extend to the far wake, which is required for the understanding of the influence of rotor wakes on the operation of other aircraft.

All the literature found relating to far wake measurements related to fixed wing wakes, as described by Corsiglia et al[2], Vicroy et al[3] and many others.

The objective of the work presented here was to determine the intermediate wake vortex characteristics of a rotor. This was to be done in terms of circulation distribution. The detailed wake structure near the rotor was not studied in this project.

The trailing vortices were measured using the rotating hot-wire technique described by Corsiglia et al[2].

Tests were initially carried out on a fixed wing to verify the test technique and then the same technique was used to measure the rotor wake characteristics.

Test Philosophy

The subject of this paper encompasses tests carried out in the Seven Metre Wind Tunnel (7mWT) at the CSIR. Intermediate wake measurements were carried out downstream of a rectangular wing and of a radio controlled (RC) helicopter.

The wing and RC helicopter were respectively mounted on a strut and balance at the entrance to the test section as shown in Figure 1. The forces measured by the balance provided an indication of trimmed flight and allowed flight conditions such as lift force and drag .to be determined.

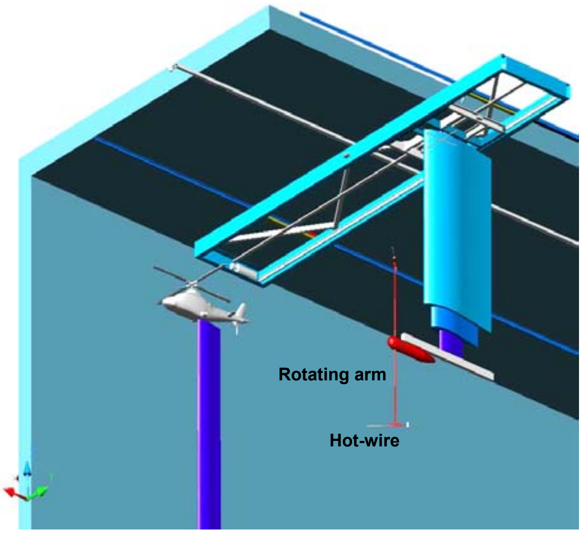

Figure 1: Schematic of the RC helicopter and traverse system in the wind tunnel

The experimental technique described by Corsiglia et al[2] details how a 3-component hot-wire can be mounted on a rotating arm and be swept rapidly through a meandering vortex to reliably measure the velocity components. This dynamic measuring technique reduces the smear effect encountered when static measurement techniques are applied to a meandering vortex.

An inclined hot-wire was mounted on the end of a rotating arm, which was in turn mounted on a traverse mechanism which could move the hot-wire within the wakes. The rotating arm was of sufficient length to make the traverse path through the vortex essentially linear. The vortex axis was assumed to be parallel to the flow axis of the wind tunnel in the plane of the measurement.

Using this rapid scanning technique alleviates the problem of meandering vortex centres. The high frequency response of the hot-wire, coupled with high speed traverses at fixed axial positions allows a series of velocity distributions to be captured in the vicinity of the vortex axis as the vortex meanders across the path of the hot-wire traverse.

Measurements were taken on the advancing side of the rotor and on one side of the wing.

Table 1: Geometric details and test conditions

Wind Tunnel	Test section	7.5 m ◊ 6.5 m
	Configuration	Open atmospheric
	V∞ (test speeds)	From 12 m/s to 22 m/s
Wing	Aspect Ratio, AR	6
	Span, b	1200 mm
	Chord, c	200 mm
	Section	NACA 0012
	α	8∞to 12∞
Rotor	Diameter = d	1337 mm
	Power	1.6 hp OS 50 methanol
	Scale	Size 46 RC model
	Chord = c	48 mm
	Rotational speed, RPM	~1200 for most flight cases
Traverse	X-component	~10000 mm
	Y-component	~6000 mm
	Z-component	~4500 mm
Rotator	Arm radius	985 mm
	Rotational frequency	1 Hz

Apparatus and Procedure

A general view of the installation (Figure 2) shows the wing installed in the 7.5 m x 6.5 m wind tunnel.

Table 1 lists the dimensions of the wing and rotor. The untwisted wing had a constant chord with square tips and a flat central section allowing for the wing/balance block attachment.

The RC helicopter was a scaled Agusta 109 with a fully articulated four bladed main rotor hub, as seen in Figure 3. The untwisted rotor blades have a constant chord of 48 mm up to 94% radius followed by a linear taper to a chord of 20 mm. The helicopter was powered by a glow plug motor of approximately 1.6 hp. Fuel was supplied by a header tank arrangement located outside of the test section.

The helicopter model was equipped with a tachometer and potentiometer to measure rotor speed and blade azimuth position. Main rotor speed was not constant and was a function of collective angle setting, which was connected to the throttle.

The earthed part of the balance was attached to a variable pitch mechanism, which allowed for the required 8∞and 12∞pitch in the case of the wing and the active control required during trimmed flight for the helicopter. This pitch control mechanism was mounted on top of a stiff faired vertical 4 m strut centrally located in the test section inlet.

An integral overhead XYZ traverse system (Figure 1) was used to support and position the rotating hot-wire.

Figure 2: NACA 0012 wing and traverse set-up with hot-wire on the rotator on the right

Instrumentation, Data Acquisition and Control Systems

The hot-wire rotator was powered using a stepper motor and toothed belt arrangement. The signals from the 3 hot-wire components were passed through slip rings to the data acquisition system. Rotational speed and azimuth position of the probe was determined using a potentiometer. Rotational speed was made an appropriate ratio of the tunnel test speed to effectively achieve a resultant flow parallel to the probe axis, which was inclined at 15∞to the tunnel axis. This allowed the full measurement range of the hot-wire to be used for measurement of the transients caused by the trailing vortex field.

Figure 3: Helicopter four bladed fully articulated hub

A 1000 Hz low pass filter was applied to the hot-wire signals which were acquired simultaneously with the potentiometer signal at a rate of 1024 Hz for the wing measurements and 2048 Hz for the rotor measurements.

The voltage data from the hot-wires was sent to the processing PC (Personal Computer) via local area network. The hot-wire data was reduced and velocity vector components were displayed in real time. This real time feedback allowed appropriate positioning of the traverse system for the hot-wire to traverse the vortex, thereby increasing the probability of vortex core penetrations.

A computer controlled the RC helicopter by supplying analogue control signals to control channels on the radio which were transmitted to the helicopter. The model was free to roll and was trimmed to a specified roll angle, using lateral cyclic. A strain gauge balance measured the aerodynamic forces on the model and the fuselage pitch and roll angles were measured by potentiometers. Software control loops used feedback from the balance and attitude potentiometers.

Calibrations

The hot-wire was first calibrated to obtain the overall calibration coefficients for the probe geometry, as described by Lekakis et al[5]. This was performed in the CSIRís calibration tunnel.

It was found that a multi-parameter 4th order polynomial characterised the calibration data set reasonably accurately for all vectors within a cone of 15∞of the probe axis. The vector could be obtained directly without further analysis of multiple solution options. Outside this 15∞ cone, however, the accuracy of this approach rapidly deteriorated.

Improved accuracy was achieved by splitting the approach vector domain into sectors delineated by the relative magnitude and ratios of the effective velocities of each wire. In this way six approach vector sectors were defined outside the central vector approach cone. A multi-parameter 4th order polynomial characterisation of the calibration data was performed for each sector, yielding a large matrix of coefficients. The measured velocity vector was determined by extracting the correct section of the calibration matrix applicable to the relevant defined flow region applicable to the measurements. The calibration matrix was generated using effective cooling velocities calculated for each wire and not the wire signals themselves. In this way the matrix was applicable for any settings on the system in terms of overheat ratios and different wires, provided the raw signals could be converted to effective cooling velocities. The orientation of each of the 3 wires was required and this was determined from photographs. The angles of the 3 wires deviated significantly from the designed orthogonal arrangement. Using this information, the calibration data was used to generate the appropriate wire parameters to allow the effective cooling velocity to be determined from combinations of the normal and tangential velocity components. This allowed the effective cooling velocity calibrations to be made in the wind tunnel with a known approach vector, without positioning each wire normal to the flow. The effective cooling velocity is;

$$V_{eff}^2 = V_N^2 + k^2 V_T^2$$

The probe was calibrated in the wind tunnel before each test to determine the effective velocity calibration coefficients for each wire. This was done by moving the probe into an area free of obstruction in the tunnel free stream. The probe rotator was spun to provide the appropriate wind vector onto the probe axis at various tunnel speeds and data was recorded for the tunnel and probe. The normal and tangential velocity components were calculated for each wire using the geometrical data for the probe, determined from the initial calibration exercise in the calibration wind tunnel, from which the effective cooling velocities were calculated. The effective cooling velocity calibration coefficients were generated and used, in conjunction with the probe calibration matrix, for the vortex scans which followed. Sensitivity of the calibration to tunnel temperature was reduced through the process of calibrating before each run.

Data Acquisition, Control and Post-processing Software

A model flight control program controlled the wing and the RC helicopter on the balance at the required trimmed flight condition in the wind tunnel. The program did this by taking measurements of balance loads and model attitudes. Control loops, with feedback from the balance and potentiometers, were written for the main rotor collective, longitudinal cyclic, lateral cyclic and model pitch. A heading lock gyro actively controlled the tail rotor collective for the tests. The operator specified a desired lift load and the computer adjusted the control surfaces of the helicopter and the pitch angle to achieve trimmed flight about the specified moment reference centre.

The wing set point required only that the AoA (Angle of Attack) be adjusted. The desired pitch angle was achieved by relay control of an electric motor powering the pitch control motor on the model pitch platform. The balance block mechanism for the wing was locked in roll.

The hot-wire control program captured the data from the pressure transducer measuring the dynamic pressure of the tunnel and then synchronised the speed the rotating arm with the velocity of the free stream in the wind tunnel. Voltages on the 3-component hot-wire were recorded on all 3 channels simultaneously using a sample and hold data acquisition system. Azimuth position of the rotating arm was also measured simultaneously with the voltages from the hot-wires. To reduce the size of the acquired data files, the sector of acquisition could be ìmaskedî and the data outside this area discarded. Data was transmitted to the control PC via the local area network.

A post-processing program was compiled to enable the traces to be viewed individually. The centre of the vortex was calculated automatically or with user inputs. A trace of the tangential velocity versus the radial co-ordinate from the vortex core was generated and curve fitted.

Figure 4 shows the data when the hot-wire penetrates very close to the vortex centre which proved to be rare. Typically the penetrations were some distance from the actual centre as shown in Figure 5. The two right hand curves show the tangential velocity plotted against radial co-ordinate in normal scale and log scale, for which the data mirrored. Both curves show the curve fitted by a polynomial and the actual measured data, which can be used for further processing. When there is little data in the core region the vortex may not be characterised completely. The penetrations closest to the core were used for further analysis.

Test Procedure

The hot-wire rotator was moved to the required measurement plane behind the wing or rotor. The wing or rotor was set at a specified lift and the hot-wire rotator was positioned so that the probe traversed the wake vortex with the axis of rotation nominally in the same horizontal plane as the vortex axis. The real time display of the velocity vectors (Figure 4) made the vortex encounters obvious. It was clear that some rotations moved through the core while others missed as the vortex meandered laterally in the flow stream. Vertical meander was captured as this was in the same direction as the probe rotation. As described earlier, only close core penetrations were selected for further processing. Run data was recorded continuously for 50 to 100 rotations at each station downstream of the wing or rotor.

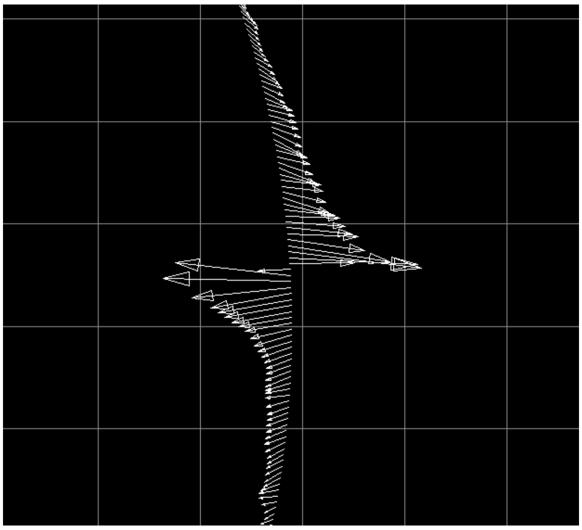

Figure 4: Typical velocity vector plot through the centre of the wing vortex

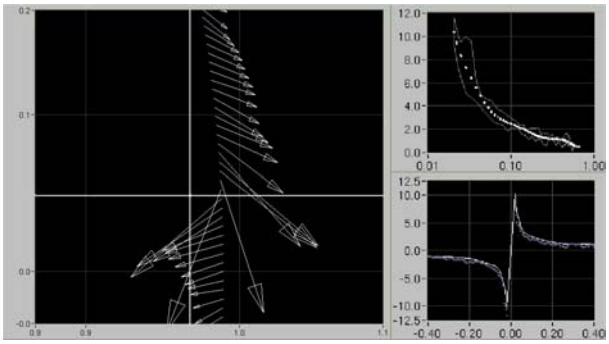

Figure 5: Example of a non-core wing vortex penetration

Velocity Distributions

The velocity components relative to the rotating probe axis were obtained from the probe calibration. These velocity components were then transformed to the non-rotating coordinate system of the wind tunnel. The tangential velocity relative to the vortex centre was determined by the vector construction, to locate vortex centre using velocity components measured along the probe traverse path, as described by Corsiglia et al[2].

Results

Traces of Hot-wire Signals for the Wing

The continuous trace of the output of all three of the hot-wire components is shown in Figure 6 as the probe moved through the core of the wing vortex. The signal to noise ratio is good and the transient event of the vortex encounter is clearly evident. The signals in the lower two traces are dominant, which is consistent with the greater lateral sensitivity produced by the orientation of these wires relative to the trailing vortex. The signal in the upper trace is sensitive to changes in pitch, which were small for vortex encounters near the centre. The lower two traces show the two peaks with the linear core region clearly.

Tangential Velocity for the Wing

The velocity vectors through the vortex is obtained from the analysis program as described earlier and a typical vector distribution through the wing vortex centre is shown in Figure 4. It can be seen, from the short velocity vectors close to the centre, that some vectors were measured in the linear region of the core. These vectors increase rapidly in magnitude as radial distance from the centre increases, until they reach a maximum velocity, and then there is a gradual reduction in tangential velocity as the radial distance from the centre increases. These changes in velocity are occurring rapidly with increasing radial distance from the core.

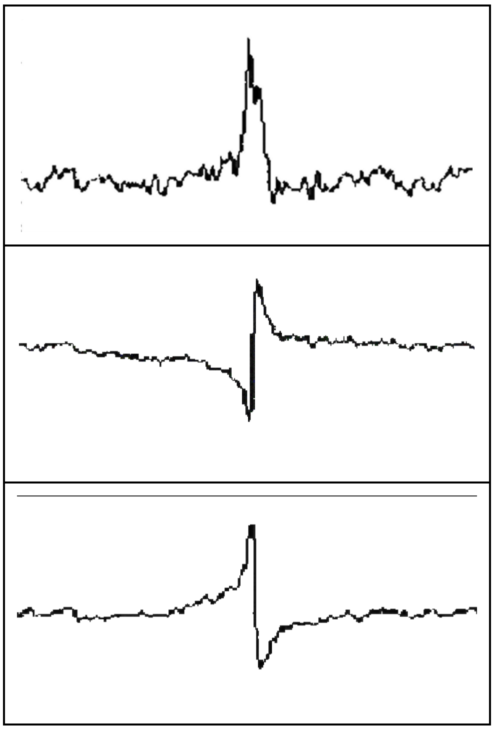

Figure 6: Raw data traces for each wire component showing penetration through the wing vortex

The resultant tangential velocities of this trace through the core of the vortex are plotted against radial position from the centre in Figure 7. This is a typical velocity profile as presented previously by many authors. Note the very small radial distance from the centre to the position of maximum tangential velocity. Although there are few data points in the îeyeî or core of the vortex it does appear to confirm that the velocity distribution is linear here, which is analogous to solid body rotation as described by Nielsen and Schwind[6].

The maximum tangential velocity and its radial location were obtained for each trace of the hot-wire through the trailing vortex for the wing. Measurements from various repeated runs were selected as having traversed close to the centre of the vortex and are shown in Figure 8. All these traces are for the same lift, speed and downstream location.

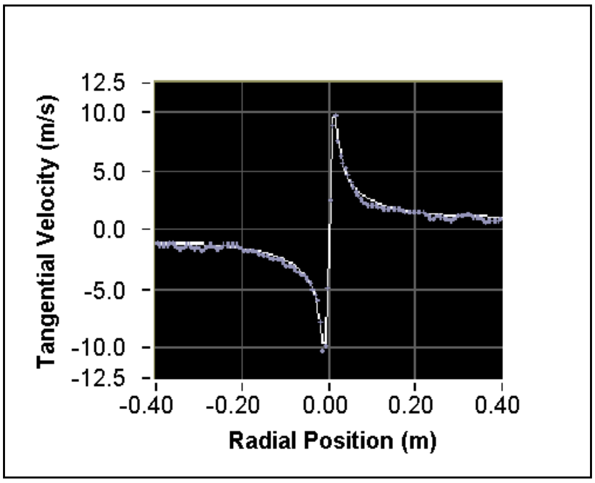

Figure 7: Resultant tangential velocity profile versus radial position through the wing vortex

The typical non-dimensionalised circulation results for the wing at 12∫ angle of attack are shown in Figure 9. Once again this is a familiar profile as shown by others such as Corsiglia et al[2] and Hoffmann and Joubert[7].

Vortex Description for the Wing

The data shown in Figure 4 to Figure 9 indicates that the test technique is appropriate and that the rotating hot-wire adequately captures the trailing vortex of the wing. For further verification, this data is now compared with data obtained by other authors.

Nielsen and Schwind[6] and earlier experiments performed by Hoffmann and Joubert[7] describe a turbulent vortex based on an analogy between turbulent vortices and turbulent boundary layer theory. From this, the vortex is divided into three regions as one moves outwards from the centre of the vortex, the core, the logarithmic region and the defect region.

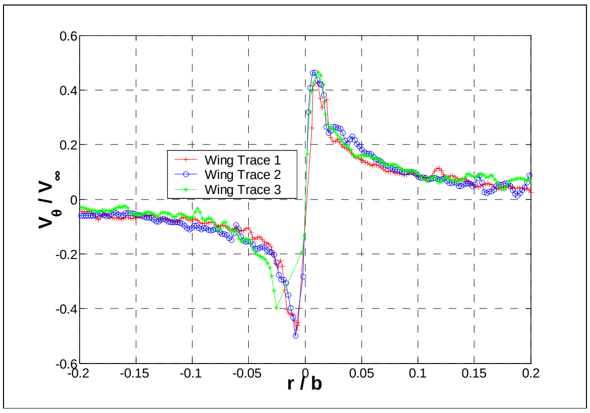

Figure 8: Multiple traces of tangential velocity distributions for the wing at $\alpha = 12$∞; $V\infty = 19$ m/s, at 10 m downstream

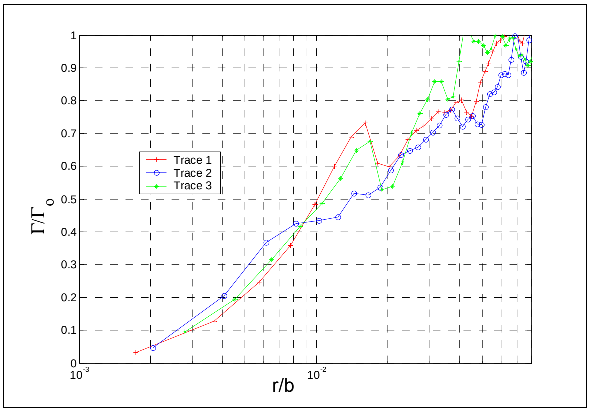

Figure 9: Circulation distributions for the wing at $\alpha =$ 12∞

Corsiglia et al[2] rewrote the equations formulated by Nielsen and Schwind[6] in a form better suited to extract empirical constants as:

$$\text{Core region:}\quad \frac{\Gamma}{\Gamma_0} = A\left(\frac{r}{b}\right)^2 \qquad (1)$$

$$\text{Logarithmic region:}\quad \frac{\Gamma}{\Gamma_0} = B\ln\left(\frac{r}{b}\right) + C \qquad (2)$$

$$\text{Defect region:}\quad \ln\left(1 - \frac{\Gamma}{\Gamma_0}\right) = D\left(\frac{r}{b}\right) + E \qquad (3)$$

Total circulation for a wing is calculated using the following:

$$\Gamma_0 = \frac{1}{2} C_L V_\infty c \qquad (4)$$

For a wing this can be rewritten to include lift,

$$\Gamma_0 = \frac{L}{(\rho V_\infty b)} \qquad (5)$$

The terms for circulation and radial position at the point of maximum tangential velocity can then be determined as follows:

$$\frac{\Gamma_1}{\Gamma_0} = B \qquad (6)$$

and

$$\frac{r_1}{b} = e^{(1-C/B)} \qquad (7)$$

The raw data for the vortex measurements for the wing at $\alpha = 12°$, $V_\infty = 19$ m/s and at 10 m downstream of the wing are again shown in Figure 10. The logarithmic region is used to determine the constants B and C in Equation 2.

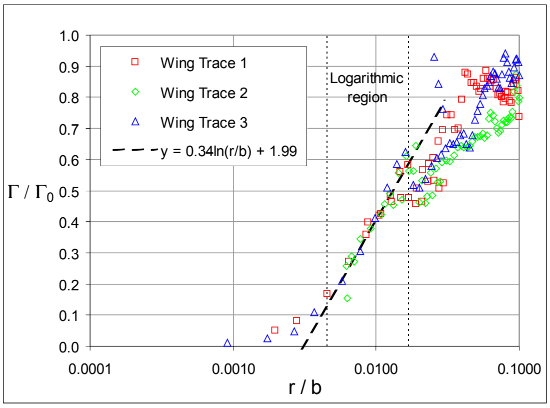

Figure 10: Determination of constants in Equation 2 for the wing trailing vortex

Circulation in the defect region is difficult to obtain due to scatter, as similarly found by Corsiglia et al[2], and Hoffmann and Joubert[7]. As the outer regions of the vortex are approached, the vortex is more sensitive to ambient conditions and more scatter is experienced in the measurements.

Nielsen and Schwind[6] defined the turbulent vortex, based on the data from Hoffmann and Joubert[7] as follows:

Core region: $$\frac{\Gamma}{\Gamma_1} = 1.83\left(\frac{r}{r_1}\right)^2 \qquad (8)$$

Logarithmic region: $$\frac{\Gamma}{\Gamma_1} = 0.928\ln\left(\frac{r}{r_1}\right) + 1 \qquad (9)$$

Defect region: $$(\Gamma_0 - \Gamma)/\Gamma_1 = 4.43e^{-4.8r/r_0} \qquad (10)$$

Once constants B and C were determined for the data as shown in Figure 10 and the values for Γ_1 and r_1 determined from Equations 6 and 7, the turbulent vortex could be defined by Equations 8 to 10 (the Nielsen and Schwind[6].model). Figure 11 shows the calculated core and log regions for the wing at $\alpha = 12°$ and the model is seen to be appropriate. The fitted curve for the defect region is not shown.

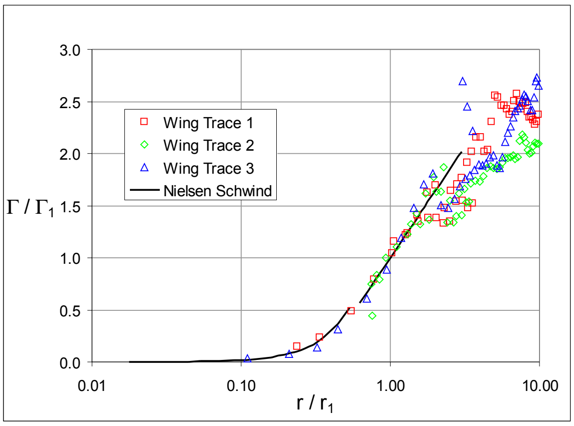

Figure 11: Nielsen and Schwind fit of circulation for the core and logarithmic regions for the wing vortex

Traces of Hot-wire Signals for the Rotor

The transient event of traversing the rotor trailing vortex is shown in Figure 12. Evidence of the vortex encounter has all but disappeared from the upper trace. The lower two traces exhibit greater changes, however, the relative magnitude is significantly lower than for the case of the wing trailing vortex encounter.

There are clearly lower velocities in the rotor trailing vortex and this results in a lower signal to noise ratio. In addition, the primary transient appears to be accompanied by secondary transients that are absent in the case of the wing. This indicates the much greater turbulence in the rotor flow, which may be expected, as the trailing vortex of the rotor stems from discreet vortices from each of the blades.

Tangential Velocity for the Rotor

A typical velocity vector trace for the rotor is shown in Figure 13 and Figure 14. There is a marked difference between the velocity vectors through the rotor trailing vortex compared to the wing trailing vortex (Figure 4). The rates of change of tangential velocity with radial distance are much more gradual for the rotor and the maximum tangential velocity is lower. Many individual disturbances are evident across the vortex and these were found to be characteristic of the rotor vortex. These are thought to be due to the interaction of the individual shed vortices from each rotor blade with the developing main trailing vortex.

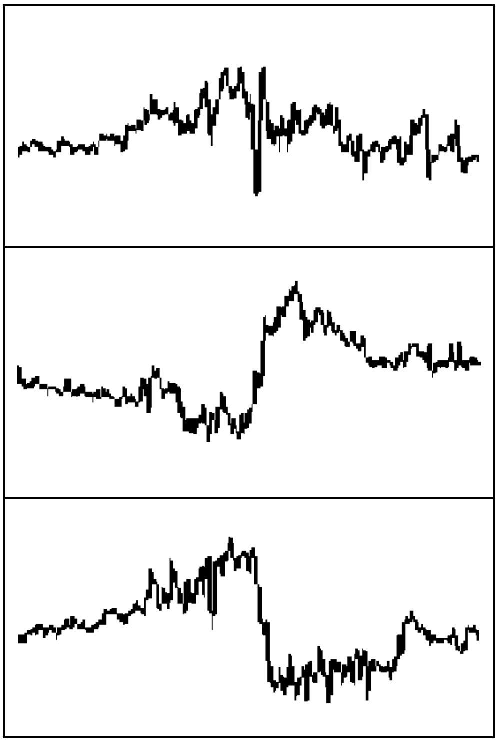

Figure 12: Raw data traces for each wire component showing penetration through the vortex core of the rotor wake

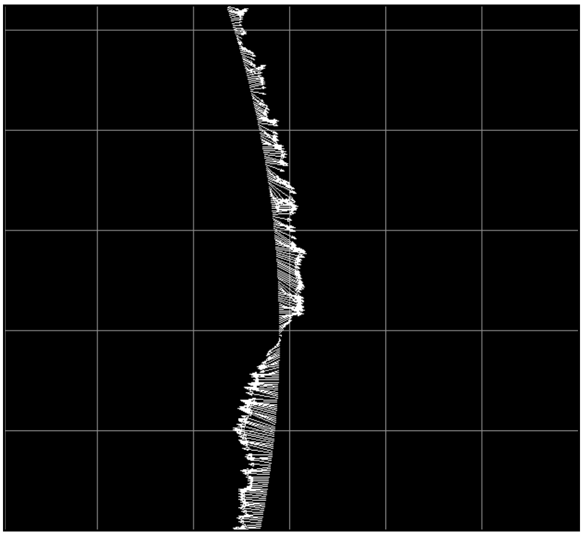

Figure 13: Typical velocity vector plot through the rotor trailing vortex

The radial distance from the vortex centre to the position of maximum tangential velocity is also much larger for the rotor vortex, as seen in Figure 15, and a linear core region is not clearly visible.

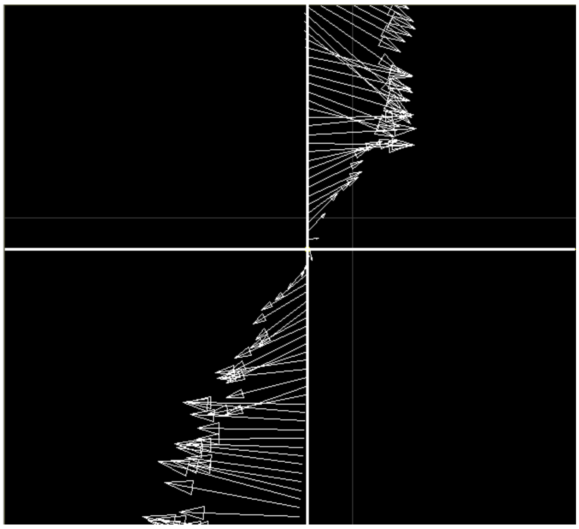

Figure 14: Velocity vector plot through core of rotor trailing vortex

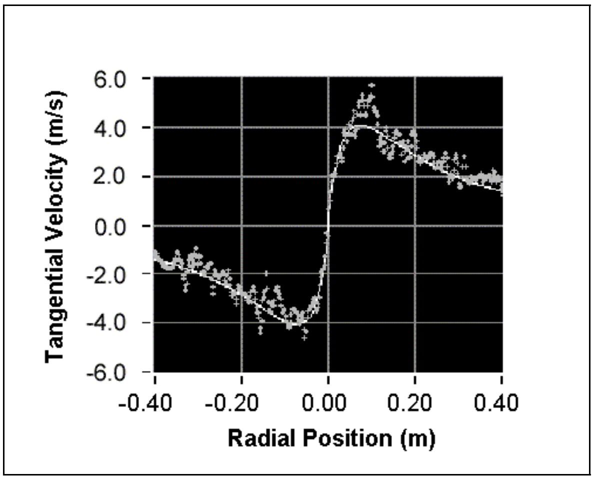

Figure 15: Tangential velocity profile through the rotor vortex (raw data and polynomial fit)

Figure 16. shows a comparison of the rotor and wing tangential velocity distributions through the trailing vortices for similar lifts, speeds and downstream distance. The significantly lower tangential velocities for the rotor trailing vortex compared to the wing trailing vortex is obvious.

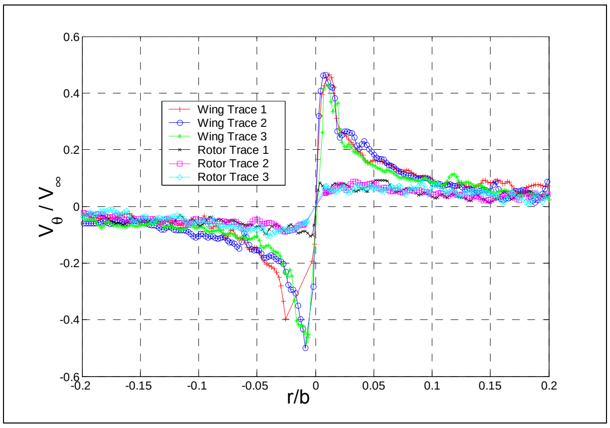

Figure 16: Comparisons between wing and rotor tangential velocities at similar lift, speed and downstream distance

Vortex Description for the Rotor

The total circulation was then calculated for the rotor as it was for the wing in Equation 5. In the case of a helicopter rotor, Johnson[8] suggests that, simplistically, the rotor can be considered to be a circular wing. Equation 5 can then be re-written for the rotor as:

$$\Gamma_0 = \frac{L}{(\rho V_\infty d)} \qquad (11)$$

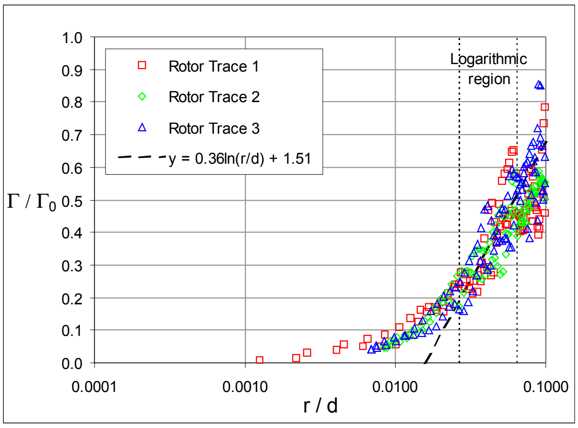

Figure 17: Defining logarithmic region for circulation, to calculate constants in Equation 2 for the rotor trailing vortex

The raw data for the rotor vortex measurements at $V_\infty = 19$ m/s and at 10 m downstream of the rotor are shown in Figure 17 for the same lift as the wing. The logarithmic region for the rotor vortex is used to define the constants B and C for Equation 2. Equation 2, denoted by the dashed line, defines the logarithmic region and the equation for this line is given on Figure 17. The fact that the logarithmic region of the rotor data occurs at larger radial positions is indicative of the larger radial location of the maximum velocity for the rotor vortex relative to that for the wing depicted in Figure 10. The logarithmic region is however similar to that of the wing as can be seen for the similar values of B as recorded in Table 2. The difference between the two vortices therefore lies mainly in the difference in the vortex structure from the centre of the vortex to the position of maximum tangential velocity.

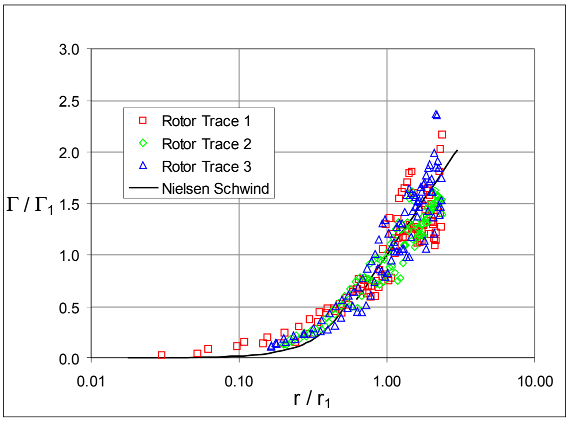

Figure 18: Nielsen and Schwind fit for circulation for the core and logarithmic regions for the wing and rotor

Table 2: Comparative constants and calculated values for the Nielsen and Schwind fit for circulation for the trailing vortex definition for the wing and rotor

Symbols	Wing	Rotor
b or d	1.200	1.337
B	0.34	0.36
C	1.99	1.51
Γ_0	1.33	1.16
Γ_1	0.46	0.42
r_1	0.010	0.056
Corsiglia et al[2],		
B	0.44	
C	2.24 to 2.54	

The values of B and C for the rotor were used to define the core and the logarithmic regions using the model developed by Nielsen and Schwind[6]. This curve is shown in Figure 18 with the experimental data. The model does not characterise the core region of the rotor trailing vortex as well as it does the core region of the wing trailing vortex (Figure 11). The model underestimates the actual circulation in the rotor vortex core region.

The values for r_1 in Table 2 indicate that the position of maximum tangential velocity in the rotor vortex occurs at a radius that is 5 to 6 times greater than for the wing vortex. This correlates with the tangential velocity differences shown in Figure 16 where the maximum tangential velocity for the rotor vortex is 5 to 6 times less than for the wing vortex.

From Figure 12 to Figure 18 it can be seen that the characteristic trailing vortex of the rotor differs significantly from that of the trailing vortex of the wing in terms of tangential velocities, core radius and data uniformity.

It is thought that the fluctuations evident in the velocity vector traces of the rotor trailing vortex are the result of discreet rotor blade trailing vortices that have not merged completely to form a single discreet trailing vortex within the measurement domain for these tests. The roll up process of the individual blade trailing vortices into the dominant rotor trailing vortex is thought to cause the discrepancy between the Nielsen and Schwind[6] model and the core region of the rotor trailing vortex.

Conclusions

The test technique employed was accurate enough to compare the results of trailing vortex characteristics of a wing with previously published results and with a RC model helicopter rotor.

The maximum tangential velocities measured in the trailing vortex of the rotor were 5 to 6 times lower than those measured for the wing for similar conditions of lift, velocity and downstream distance. The radial location from the vortex centre of the maximum tangential velocity for the rotor is also 5 to 6 times larger than that for the wing.

Good correlation was obtained between the Nielsen and Schwind[6] model for turbulent vortices and the wing trailing vortex.

By considering the rotor disc as a circular wing, good correlation was also achieved between the Nielsen and Schwind[6] model for the logarithmic region of the rotor trailing vortex however the core region was not well described.

References

[1] Ghee, T A, Berry, J D, Zori, L A J, Elliot, J W; *Wake Geometry Measurements and Analytical Calculations on a Small-Scale Rotor Model*; NASA TP3584, ATCOM TR-96-A-007, August 1996

[2] Corsiglia, V R, Schwind, R G, Chigier, N A; *Rapid Scanning, Three-Dimensional Hot-wire Anemometer Surveys of Wing-Tip Vortices*; Journal of Aircraft, Vol. 10, No. 12, December 1973

[3] Vicroy, D D, Brandon, J, Greene, G, Rivers, R, Shah, G, Stewart, E, Stuever, R; *Characterizing the Hazard of a Wake Vortex Encounter*; AIAA paper

[4] IFA100 Instruction Manual, TSI

[5] Lekakis, I C, Adrian, R J, Jones, B G, *Measurement of velocity vectors with orthogonal and non-orthogonal triple-sensor probes,* Experiments in Fluids, Springer-Verlag, 1989

[6] Nielsen, J N and Schwind, R G, *Decay of a vortex pair behind an aircraft,* Proceedings of Symposium on Aircraft Wake Turbulence, September 1-3, 1970, Plenum Press, London, 1971

[7] Hoffmann, E R and Joubert, P N, *Turbulent Line Vortices*, Journal of Fluid Mechanics, Vol. 16, Pt. 3, July 1963, pp. 395-411

[8] Johnson, W, *Helicopter Theory,* Princeton University Press, 1980